Atmospheric
Chemistry
and Physics
Discussions
Open Access
EGU

OBSERVATIONS OF HIGHLY OXIDISED MOLECULES AND PARTICLE NUCLEATION IN THE ATMOSPHERE OF BEIJING

James Brean[1], Roy M. Harrison[1*†], Zongbo Shi[1]
David C.S. Beddows[1], W. Joe F. Acton[2] and
C. Nicholas Hewitt[2]

[1]Division of Environmental Health and Risk Management,
School of Geography, Earth and Environmental Sciences
University of Birmingham
Edgbaston, Birmingham B15 2TT
United Kingdom

[2]Lancaster Environment Centre
Lancaster University, Lancaster LA1 4YQ
United Kingdom

---

* To whom correspondence should be addressed.
Tele: +44 121 414 3494; Fax: +44 121 414 3709; Email: r.m.harrison@bham.ac.uk

†Also at: Department of Environmental Sciences / Center of Excellence in Environmental Studies, King Abdulaziz University, PO Box 80203, Jeddah, 21589, Saudi Arabia

Atmospheric
Chemistry
and Physics
Discussions
Open Access
EGU

20 **ABSTRACT**

21 Particle nucleation is one of the main sources of atmospheric particulate matter by number, with new

22 particles having great relevance for human health and climate. Highly oxidised multifunctional

23 organic molecules (HOMs) have been recently identified as key constituents in the growth, and,

24 sometimes, in initial formation of new particles. While there have been many studies of HOMs in

25 atmospheric chambers, flow tubes and clean environments, analyses of data from polluted

26 environments are scarce. Here, measurements of HOMs and particle size distributions down to small

27 molecular clusters are presented alongside VOC and trace gas data from a campaign in Beijing. Many

28 gas phase HOMs have been characterised and their temporal trends and behaviours analysed in the

29 context of new particle formation. The HOMs identified have a comparable degree of oxidation to

30 those seen in other, cleaner, environments, likely due to an interplay between the higher temperatures

31 facilitating rapid hydrogen abstractions and the higher concentrations of NOx and other $RO_2^.$

32 terminators ending the autoxidation sequence more rapidly. Our data indicate that alkylbenzenes,

33 monoterpenes, and isoprene are important precursor VOCs for HOMs in Beijing. Many of the C_5 and

34 C_{10} compounds derived from isoprene and monoterpenes have a slightly greater degree of average

35 oxidation state of carbon compared to those from other precursors. Most HOMs except for large

36 dimers have daytime peak concentrations, indicating the importance of $OH^.$ chemistry in the

37 formation of HOMs, as O_3 is lower on the days with higher HOM concentrations; similarly, VOC

38 concentrations are lower on the days with higher HOM concentrations. The daytime peaks of HOMs

39 coincide with the growth of freshly formed new particles, and their initial formation coincides with

40 the peak in sulphuric acid vapours, suggesting that the nucleation process is sulphuric acid-dependent,

41 with HOMs contributing to subsequent particle growth.

42

43

Atmospheric
Chemistry
and Physics
Discussions

1.   INTRODUCTION

Atmospheric particle nucleation, or the formation of solid or liquid particles from vapour phase

precursors is one of the dominant sources of global aerosol by number, with primary emissions

typically dominating the mass loadings (Tomasi et al., 2016). New particle formation (NPF) or the

secondary formation of fresh particles is a two-step process comprising of initial homogeneous

nucleation of thermodynamically stable clusters and their subsequent growth. The rate of growth

needs be fast enough to out-compete the loss of these particles by coagulation and condensation

processes in order for the new particles to grow, and hence NPF is a function of the competition

between source and sink (Gong et al., 2010). New particle formation has been shown to occur

across a wide range of environments (Kulmala et al., 2005). The high particle load in urban

environments was thought to suppress new particle formation until measurements in the early 2000s

(McMurry et al., 2000; Shi et al., 2001; Alam et al., 2003), with frequent occurrences observed even

in the most polluted urban centres. NPF events in Beijing occur on about 40% of days annually,

with the highest rates in the spring (Wu et al., 2007, 2008; Wang et al., 2016). Chu et al. (2019)

review the many studies of NPF which have taken place in China and highlight the need for long-

term observations and mechanistic studies.

NPF can lead to production of cloud condensation nuclei (CCN) (Wiedensohler et al., 2009; Yu and

Luo, 2009; Yue et al., 2011; Kerminen et al., 2012) which influences the radiative atmospheric

forcing (Penner et al., 2011). A high particle count, such as that caused by nucleation events, has

been shown to precede haze events in environments such as Beijing (Guo et al., 2014). These events

are detrimental to health and quality of life. The sub-100 nm fraction of particles to which new

particle formation contributes to is often referred to as the ultrafine fraction. Ultrafine particles

(UFPs) pose risks to human health due to their high number concentration. UFPs exhibit gas-like

behaviour and enter all parts of the lung before penetrating into the bloodstream (Miller et al.,

2017). They can initiate inflammation via oxidative stress responses, progressing conditions such as

70 atherosclerosis and initiating cardiovascular responses such as hypertension through to myocardial

71 infarction (Delfino et al., 2005; Brook et al., 2010).

72

73 Highly oxidised multifunctional molecules (HOMs), organic molecules with O:C ratios >0.6, are

74 the result of atmospheric autoxidation and have recently been subject to much investigation, in part

75 because the extremely low volatilities arising from their high O:C ratios favour their condensation

76 into the particulate phase. HOMs are most well characterised as the product of oxidation of the

77 biogenic monoterpenoid compound α-pinene (Riccobono et al., 2014; Tröstl et al., 2016; Bianchi et

78 al., 2017). Although globally, BVOC concentrations far exceed aromatic VOC concentrations by

79 approximately a factor of 10, in the urban environment the aromatic fraction is far more significant.

80 Formation of HOMs from aromatic compounds has been demonstrated in laboratory studies and

81 these have been hypothesised to be large drivers of NPF in urban environments (Wang et al., 2017;

82 Molteni et al., 2018; Qi et al., 2018). The formation of HOMs through autoxidation processes

83 begins with the reaction of VOCs with OH$^.$, O$_3$ or NO$^.$$_3$; formation of a peroxy radical (RO$^.$$_2$) is

84 followed by rapid O$_2$ additions and intra-molecular hydrogen abstractions (Jokinen et al., 2014;

85 Rissanen et al., 2014; Kurtén et al., 2015). Furthermore, generation of oligomers from stabilised

86 Criegee intermediates arising from short chain alkenes has been hypothesised as a contributor of

87 Extremely Low Volatility Organic Compounds (ELVOCs) and Low Volatility Organic Compounds

88 (LVOCs) (Zhao et al., 2015). The result of the large size and numerous oxygen-containing

89 functionalities in all of these compounds is a low vapour pressure, and therefore they make a

90 significant contribution to particle growth (Tröstl et al., 2016), although the contribution of HOMs

91 to the initial molecular clusters is still debated (Kurtén et al., 2016; Elm et al., 2017; Myllys et al.,

92 2017).

93

94 Recent technological advances have facilitated insights into the very first steps of nucleation which

95 were previously unseen, with mass spectrometric techniques such as the Atmospheric Pressure

Atmospheric
Chemistry
and Physics
Discussions

Open Access

EGU

96   Interface Time of Flight Mass Spectrometer (APi-ToF) and its chemical ionisation counterpart (CI-

97   APi-ToF) allowing for high mass and time resolution measurements of low volatility compounds

98   and molecular clusters. Diethylene glycol based particle counters, such as the Particle Size

99   Magnifier (PSM) allow for measurements of particle size distributions down to the smallest

100   molecular clusters nearing 1 nm. Recent chamber studies have elucidated the contribution of

101   individual species to particle nucleation, ammonia and amines greatly enhancing the rate of sulfuric

102   acid nucleation (Kirkby et al., 2011; Almeida et al., 2013). In these studies, HOMs have been

103   identified, formed through autoxidation mechanisms (Schobesberger et al., 2013; Riccobono et al.,

104   2014; Ehn et al., 2014). These are key to early particle growth (Tröstl et al., 2016) and can nucleate

105   even in the absence of sulfuric acid in chambers (Kirkby et al., 2016) and in the free troposphere

106   (Rose et al., 2018). In this paper, we report the results of HOM and particle size measurements

107   during a summer campaign in Beijing, China.

108

109   **2.   DATA AND METHODS**

110   **2.1.   Sampling Site**

111   Sampling was performed as part of the APHH-Beijing campaign, a large international collaborative

112   project examining emissions, processes and health effects of air pollution. For a comprehensive

113   overview of the programme, see Shi et al. (2018). All sampling was conducted across a one month

114   period at the Institute for Atmospheric Physics (IAP), Chinese Academy of Sciences, Beijing

115   ($39^o58.53$'N, $116^o22.69$'E). The sampling was conducted from a shipping container, with sampling

116   inlets 1-2 metres above ground level, the nearest road being 30 metres away. Meteorological

117   parameters (wind speed, wind direction, relative humidity (RH) and temperature) were measured at

118   the IAP meteorological tower, 20 metres away from the sampling site, 30 metres from the nearest

119   road at a height of 120 metres. Data was continuously taken from the CI-APi-ToF during a two

120   week period, but due to data losses only five days of data is presented here. Particle size distribution

121   measurements were taken during a 33 day period from 24/05/2017 – 26/06/2017.

Atmospheric
Chemistry
and Physics
Discussions

2.2   Chemical Ionisation Atmospheric Pressure Interface Time of Flight Mass

        Spectrometry

The Aerodyne Nitrate Chemical Ionisation Atmospheric Pressure Interface Time of Flight Mass

Spectrometer (CI-APi-ToF) was used to make measurements of neutral oxidised organic

compounds, sulfuric acid and their molecular clusters at high time resolution with high resolving

power. The ionization system charges molecules either by forming an adduct with NO_3^-, or by

proton transfer to NO_3^-. The former occurs largely with species with two hydrogen bond donor

groups, such as organics with two or more hydroxyl or hydroperoxyl functionalities (Hyttinen et al.,

2015), with hydroperoxyl being the more efficient hydrogen bond donor (Møller et al., 2017).

Proton transfer occurs with molecules with great proton affinity such as sulfuric acid, although

clustering with sulfuric acid does occur. This instrument has been explained in great detail

elsewhere (Junninen et al., 2010; Jokinen et al., 2012), but briefly the front end consists of a

chemical ionisation system where a 10 Lpm sample flow is drawn in through the 1 metre length 1"

OD stainless steel tubing opening. A 3 sccm flow of a carrier gas (N_2) containing nitrate ions

generated by the X-ray ionisation of nitric acid vapour is run parallel and concentric to the sample

flow in an ion reaction tube. The nitrate ions will then charge molecules either by clustering or

proton transfer. The mixed flows travelling at 10 sLm enter the critical orifice at the front end of the

instrument at 0.8 sLm and are guided through a series of differentially pumped chambers before

reaching the ToF analyser. Two of these chambers contain quadrupoles which can be used to select

greater sensitivity for certain mass ranges, and the voltages across each individual chamber can be

tuned to maximise sensitivity and resolution for ions of interest. Mass spectra are taken at a

frequency of 20 kHz but are recorded at a rate of 1 Hz. All data analysis was carried out in the

Tofware package in *Igor Pro 6* (Tofwerk AG, Switzerland). A seven point mass calibration was

performed for every minute of data, and all data was normalised to signal at 62, 80 and 125 *m/Q* to

account for fluctuations in ion signal, these masses representing NO_3^-, $H_2ONO_3^-$ and $HNO_3NO_3^-$

respectively. The nitrate-water cluster is included as the presence of many nitrate-water clusters of

148   the general formula $(H_2O)_x(HNO_3)_yNO_3^-$ were found, where $x = (1, 2, 3... 20)$ and $y = (0, 1)$. No

149   sensitivity calibration was performed for these measurements, and so all values are reported in

150   signal intensity, ions/s. Due to the high resolving power of the CI-APi-ToF system, multiple peaks

151   can be fit at the same unit mass and their molecular formulae assigned. These peaks follow the

152   general formula $C_xH_yO_zN_w$ where $x = 2−20$, $y = 2−32$, $z = 4−16$ and $w = 0−2$, spanning from small

153   organic acids like oxalic and malonic acid through to large dimers of oxidised monoterpene $RO_2^{\cdot}$

154   radicals such as $C_{20}H_{31}O_9N$. Beyond 500 m/Q, peak fitting and assignment of compositions

155   becomes problematic as signal decreases, mass accuracy decreases, and the total number of

156   chemical compositions increases, so peaks above the C_{20} region have not been assigned, and a

157   number of peaks have been unassigned due to this uncertainty (Cubison and Jimenez, 2015). As

158   proton transfer mostly happens with acids, and nearly all HOM molecules will be charged by adduct

159   formation it is possible to infer the uncharged formula; therefore all HOMs from here onwards will

160   be listed as their uncharged form.

161

2.3.   Size Distribution Measurements

163   Two Scanning Mobility Particle Sizer (SMPS) instruments measured particle size distributions at

164   15 minute time resolution, one LongSMPS (TSI 3080 EC, 3082 Long DMA, 3775 CPC, TSI, USA)

165   and one NanoSMPS (3082 EC, 3082 Nano DMA, 3776 CPC, TSI, USA) measuring the ranges 4-65

166   nm and 14-615 nm respectively. A Particle Size Magnifier (A10, Airmodus, FN) linked to a CPC

167   (3775, TSI, USA) measured the sub-3 nm size fraction. The PSM was run in stepping mode,

168   operating at four different saturator pressures to vary the lowest size cut-off of particles that it will

169   grow (this cut-off is technically a point of 50% detection efficiency) of <1.30, 1.36, 1.67 and 2.01

170   nm. The instrument switched between saturator pressures per 2.5 minutes, giving a sub-2.01 nm

171   size distribution every 10 minutes. The data was treated with a moving average filter to account for

172   jumps in total particle count, and due to the similar behaviour of the two upper and two lower size

173   cuts, these have been averaged to two size cuts at 1.30 and 1.84 nm.

Atmospheric
Chemistry
and Physics
Discussions

Open Access

EGU

174 **2.4.** **Calculations**

175 The condensation sink (CS) was calculated from the size distribution data as follows:

176
$$CS = 4\pi D \sum_{d'_p} \beta_{m,d'_p} d'_p N_{d'_p} \qquad (1)$$

177

178 where D is the diffusion coefficient of the diffusing vapour (assumed sulfuric acid), and β_m is a

179 transition regime correction (Kulmala et al., 2012).

180

181 **2.5.** **Other Measurements**

182 SO_2 was measured using a 43i SO_2 analyser (ThermoFisher Scientific, USA), O_3 with a 49i O_3

183 analyser (ThermoFisher Scientific, USA) and NO_x with a 42i-TL Trace NO_x analyser

184 (ThermoFisher Scientific, USA), and a T500U CAPS NO_2 analyser (Enviro Technology Services,

185 USA). VOC mixing ratios were measured using a Proton Transfer Reaction-Time of Flight-Mass

186 Spectrometer (PTR-ToF 2000,Ionicon, Austria). Measurements of $J(O^1D)$ were carried out via filter

187 radiometers (Bohn et al., 2016) and measurements of OH, RO_2, and HO_2 concentrations were

188 carried out by Fluorescence Assay by Gas Expansion (FAGE) (Winiberg et al., 2016).

189

190 **3.** **RESULTS AND DISCUSSION**

191 **3.1.** **Characteristics of Sampling Period**

192 A total of five days of CI-API-ToF data were collected successfully, from 2017/06/21 midday

193 through 2017/06/26 midday. New particle formation events were observed on 24th June in the late

194 afternoon and 25th June at midday. Some nighttime formation of molecular clusters was seen

195 earlier in the campaign, as were several peaks to the 1.5 – 100 nm size range, likely from pollutant

196 plumes containing freshly nucleating condensable materials. The trace gases, O_3, SO_2, NO and NO_2

197 are plotted in the Figure S1. O_3 shows mid-afternoon peaks, around ~120 ppbv on the first two days

198 of the campaign, and 50-70 ppbv for the latter days. SO_2 shows a large peak, reaching 4 ppbv on

199   22/06 but <1 ppbv for the rest of campaign. NO shows strong mid-morning rush hour related peaks,

200   declining towards midday due to being rapidly consumed by O_3. NO_2 shows large traffic related

201   peaks. The sulfuric acid signal across this period as measured by NO_3^- CI-APi-ToF showed strong

202   midday peaks, with concentrations highest on 24/06/2017 and 25/06/2017. The meteorological data

203   are shown in Figure S2 alongside condensation sink (CS). The conditions were generally warm and

204   humid, with temperature reaching its maximum on 25/06/2017, with a peak hourly temperature of

205   31°C. High temperatures were seen on 21/06 and 24/06 also, of 30°C and 26°C respectively.

206

207   **3.2.   Gas Phase HOM Chemistry**

208   **3.2.1.   Bulk chemical properties**

209   For the peaks that that have had chemical formulae assigned, oxidation state of carbon, or OS_c, can

210   be used to describe their bulk oxidation chemistry. OS_c is defined as (Kroll et al., 2011)

211

$$OSc \; = \; (2 \times O{:}C) - H{:}C \quad (2)$$

213

214   This does not account for the presence of nitrate ester groups, which has been accounted for

215   previously by subtracting five times the N:C ratio (Massoli et al., 2018), under the assumption that

216   all nitrogen containing functionality is in the form of nitrate ester ($RONO_2$) groups. In Beijing,

217   multiple sources of nitrate-containing organic compounds are seen, in the forms of amines, nitriles

218   and heterocycles. The variation of oxidation state with carbon number (C_n) is plotted in Figure 1.

219   The average oxidation state of carbon in this dataset tends to decrease with an increase to C_n,

220   highest where $C_n = 5$, attributable both to high O:C and peak area for the peak assigned to

221     $C_5H_{10}N_2O_8$ at m/Q 288. $C_n = 5$ also shows the greatest distribution of oxidation states, likely due to

222   the high ambient concentration of isoprene and therefore its many oxidation products being of high

223   enough concentrations for many well resolved peaks to be seen in this dataset. $C_n = 10$ and 15 also

224   see a small increase to average oxidation number compared to their neighbours. The lower

225   oxidation state of the larger products is likely a function of two things. First and foremost, any

226   autoxidation mechanism must undergo more steps in order for a larger molecule to reach an

227   equivalent O:C ratio with a smaller one, and the equivalent O:C ratio is ultimately less likely to be

228   reached before the radical is terminated (Massoli et al., 2018). Secondly, the lower vapour pressures

229   of these larger products will lead to their partitioning into the condensed phase more readily than

230   the smaller, thus they are more rapidly lost (Mutzel et al., 2015).

231

232   The degrees of OSc observed here are similar to those seen in other environments such as during

233   the SOAS campaign in 2013 in southern United States, characterised by low NO/NO_2 and high

234   temperatures, where campaign averages of 0.3 ppb, 0.4-0.5 ppb, and 25°C respectively were

235   measured, although an additional parameter to account for nitrogen containing VOCs is included in

236   the calculation (Massoli et al., 2018). The OS_c observed in Beijing is also higher than that seen in

237   the boreal forest environment of Hyytiälä, despite extremely low NO_x concentrations, likely due to

238   low temperature conditions dominating in those conditions (Schobesberger et al., 2013). These

239   relatively similar degrees of oxidation to those seen in other, cleaner, environments are likely due to

240   an interplay between the higher temperatures facilitating rapid hydrogen abstractions (Crounse et

241   al., 2013; Praske et al., 2018; Quéléver et al., 2018) and the higher concentrations of NO_x, $HO_2^{\cdot}$, and

242   other $RO_2^{\cdot}$ molecules terminating the autoxidation sequence more efficiently.

243

244   A mass defect plot is shown in Figure 2. The band of lower mass defect is characterised by a

245   number of large peaks with high signal, for example, at m/Q 344 the ion $(NH_3)_3(H_2SO_4)_2HSO_4^-$ and

246     $(H_2O)_2(NH_3)_2(H_2SO_4)_2HSO_4^-$ at m/Q 362. Many water clusters are seen here. This clustering may

247   happen in the atmosphere, in the chemical ionisation inlet or through the critical orifice in the small

248   segmented quadrupole (SSQ) section of the instrument, and there is a weak dependence of these

249   concentrations on the SSQ pressure. The upper component of the mass defect is dominated by

250   organics, the upper end of more positive mass defect is occupied by molecules with more [1]H (mass

Atmospheric
Chemistry
and Physics
Discussions

251 defect 7.825 mDa) and ^{14}N (mass defect 3.074 mDa). The end of less positive mass defect has lower

252 ^{1}H and more ^{16}O (mass defect -5.085 mDa); alternatively put, the mass defect reflects the variation

253 in OS_c. The organic components with more positive mass defects will be more volatile than their

254 lower mass defect counterparts as they will contain fewer oxygen functionalities (Tröstl et al., 2016,

255 Stolzenburg et al., 2018). These higher volatility products may still contribute to larger size particle

256 growth. The more negative mass defect components will be those of greater O:C and therefore

257 lower volatility, LVOCs, and the yet larger and more oxidised components, ELVOCs (Tröstl et al.,

258 2016).

259

260 **3.2.2.   Diurnal trends of HOMs**

261 Temporal trends of HOMs in the urban atmosphere can throw light upon their sources and

262 behaviour in the atmosphere. Most of the HOM species peak in the daytime. These species all

263 follow a similar diurnal trend, as shown in Figure 3. Both the concentrations of O_3 and OH$^.$ are high

264 during this period (although the nitrate chemical ionisation technique is not sensitive to all OH$^.$

265 oxidation products (Berndt et al., 2015)). Figure S1 shows the time series of concentrations of NO

266 which is considered a dominant peroxy radical terminator of particular importance in the polluted

267 urban environment (Khan et al., 2015). Peroxy radicals such as HO_2 and RO_2 also typically peak

268 during daytime.   The HOM components peaking in the daytime are presumed to be the oxidation

269 products of a mixture of anthropogenic and biogenic components, such as alkylbenzenes,

270 monoterpenes and isoprene. The oxidation of monoterpenes, specifically the monoterpene α-pinene,

271 has been the subject of extensive study recently, with the O_3-initiated autoxidation sequence being

272 the best characterised (Ehn et al., 2014; Jokinen et al., 2014; Kurtén et al., 2015; Kirkby et al.,

273 2016); ozonolysis of α-pinene opens the ring structure and produces a RO$^.$$_2$ radical (Kirkby et al.,

274 2016). In the case of aromatics, OH$^.$ addition to the ring and the subsequently formed bicyclic

275 peroxy radical is the basis for the autooxidation of compounds such as xylenes and

276 trimethylbenzenes (Molteni et al., 2018; Wu et al., 2017).

Atmospheric
Chemistry
and Physics
Discussions

Open Access

EGU

277   The identified compounds have been roughly separated into several categories, each of these plotted

278   in Figure 3. The top of this graph shows the separation of components into HOM and ON

279   (organonitrate) components. The ON signal is much higher than that of the HOM, attributable in

280   part to a few ions of high signal, such as the isoprene organonitrate $C_5H_{10}N_2O_8$. A few similar

281   structural formulae are seen ($C_5H_{10}N_2O_6$, $C_5H_{11}NO_6$, $C_5H_{11}NO_7$, etc), some of which have been

282   identified as important gas phase oxidation products of isoprene under high NO_x conditions (Xiong

283   et al., 2015), and their contribution to SOA has been explored previously (Lee et al., 2016). A high

284   nitrophenol signal is also seen, $C_6H_5NO_3$. The signal for HOM compounds is less dominated by a

285   few large ions. The prevalence of ON compounds points towards the important role of NO_x as a

286   peroxy radical terminator, with the probability for the $RO_2^. + NO_x$ reaction to produce nitrate ester

287   compounds increasing with the size of the $RO_2^.$ molecule (Atkinson et al., 1982). The NO_x

288   concentrations in urban Beijing are approximately a factor of 10 higher than seen at the Hyytiälä

289   station in Finland as reported by Yan et al. (2016), and hence it is expected to be a more significant

290   peroxy radical terminator.

291

292   Despite the very large fluxes of anthropogenic organic pollutants in Beijing, biogenic emissions are

293   still an important source of reactive VOCs in the city, with abundant isoprene oxidation products

294   observed (see above), as well as monoterpene monomers ($C_{10}H_{16}O_9$, $C_{10}H_{15}O_9N$) and some dimer

295   products ($C_{20}H_{30}O_{11}$, $C_{20}H_{31}O_{11}N$). The time series of the concentrations all C_5, C_{10} and C_{20}

296   molecules is plotted in the middle panel of Figure 3, with C_5 species assumed to be isoprene

297   dominated, C_{10} and C_{20} assumed to be monoterpene dominated. Isoprene oxidation products are

298   present at higher concentrations, with abundant isoprene nitrate and dinitrate products. C_{10} products

299   show similar behaviour, with, for example, several $C_{10}H_{15}O_xN$ $x = 5-9$ compounds seen. The C_{20}

300   products seen are low in concentration, and follow the general formula $C_{20}H_xO_yN_z$, where $x =$

301    $26-32$, $y = 7-11$ and $z = 0-2$; in Figure 3 the signal for C_{20} compounds has been multiplied by a

302   factor of 50 for visibility. The low concentrations reflect the lack of RO_2^- cross reactions necessary

303   for the production of these accretion products.

304

305   Other identified peaks are plotted in the bottom panel of Figure 3. The C_2-C_4 components are

306   summed together, these being small organic acids such as malonic acid and oxalic acid, as well as

307   products such as $C_4H_7O_6N$. Malonic acid is the most prominent here, seen both as an NO_3^- adduct

308   ($C_3H_4O_4NO_3^-$) and a proton transfer product ($C_3H_3O_4^-$) at a ratio of around 2:3. The C_6-C_9

309   components are assumed to be dominated by oxidation products of alkylbenzenes such as $C_8H_{12}O_5$,

310   although fragments of other compounds, i.e., monoterpenes, can also occupy this region (Isaacman-

311   Vanwertz et al., 2018). It is assumed the majority of the signal for these peaks come from

312   alkylbenzenes. This assumption is supported by the relative ratios of the monomer $C_8H_{12}O_n$

313   compounds being similar to those seen for xylene oxidation products in previous work (Molteni et

314   al., 2018). The largest fraction, C_{11} through $C_{18,}$ includes the larger compounds, oxidation products

315   of larger aromatics, or products of the cross reaction of smaller RO_2^- radicals. Here they are grouped

316   without more sophisticated disaggregation as they all follow much the same time series, species

317   such as $C_{11}H_{11}O_8N$ following the same temporal trends as $C_{15}H_{16}O_9$ and $C_{16}H_{24}O_{12}$.

318

319   Nearly all ions with the exception of the larger compounds attributed to the cross reaction of C_{10}

320   monomers follow similar temporal patterns, with the majority of peaks occurring in the daytime.

321   This reflects the importance of the concentration of atmospheric oxidants. Some selected oxidation

322   products are plotted against their precursor VOCs in Figure 4. The concentration of isoprene is

323   plotted against the concentration of a nitrate HOM product, $C_5H_9NO_6$ (Xiong et al., 2015; Lee et al.,

324   2016), while monoterpenes are plotted against $C_{10}H_{16}O_9$ (Ehn et al., 2014; Berndt et al., 2016; Yan

325   et al., 2016; Kirkby et al., 2016; Massoli et al., 2018), and C_2-benzenes against $C_8H_{12}O_6$ (Molteni et

326   al., 2018; Wang et al., 2017). The first half of the time series shows little correlation between the

327   VOC species and the resultant oxidation products, while isoprene, monoterpenes and C_2-benzenes

328   follow their usual diurnal cycles, isoprene having the most distinct with a strong midday peak. The

329   latter two days, however, show similar and coinciding peaks in both the VOCs and HOMs - HOMs

330   show afternoon peaks on both days, and an initial shelf on the final half day. The $C_5H_9NO_6$ peak

331   follows some of the peaks of the isoprene, but not all (e.g., morning shelf of isoprene on 24/06).

332   Concentrations of isoprene do not seem to determine directly the concentration of HOM, as the day

333   with the lowest isoprene of all is the day with highest $C_5H_9NO_6$. The $C_{10}H_{16}O_9$ trace has

334   coincidental peaks with the monoterpene trace also, including two 4-hour separated simultaneous

335   peaks on 25/06. The peaks in the concentrations of C_2-benzenes are nearly synchronous with the

336   peaks in $C_8H_{12}O_6$; these exhibit a strong early afternoon peak likely due to the lack of an efficient

337   ozonolysis reaction pathway; the main oxidant of C_2-benzenes is the OH· radical. This behaviour is

338   much the same as the C_3-benzenes and their oxidation products. The concentration of precursor

339   VOC is likely a driving force in the identity and quantity of various HOM products, but not the sole

340   determinant, as while there are simultaneous peaks of VOCs and HOMs, both the condensation sink

341   and oxidant concentrations also influence HOM product concentrations.

342

343   The first half of campaign measurements is marked by an episode of low HOM concentrations. A

344   diurnal cycle still exists but it is weak. $J(O^1D)$ is used in Figure S1 as a proxy for radiation intensity,

345   and the radiation intensity is significantly lower on these prior days than it is on the 24th. No data is

346   available for the final period of measurement. Ozone is higher on the prior measurement days with

347   lower HOM concentrations (see Figure S2). It is therefore plausible that light intensity, and

348   therefore OH· concentration is one of the main drivers of HOM concentrations in Beijing.

349

350   The C_{20} compounds show no strong diurnal sequence, contrasting with other HOMs. We can

351   presume that all C_{20} compounds identified are the result of the reaction of two monoterpenoid C_{10}

352   RO·$_2$ radicals, a reasonable assumption as all identified C_{20} species follow the general formula

353   outlined for these reactions ($C_{20}H_{28-32}O_{6-16}$). The formation of C_{20} dimers is dependent upon two

354   processes, initial oxidation of monoterpenes, and RO_2-RO_2 termination. Initial oxidation is

355   contingent upon oxidant concentration, which is highest in the daytime, and $RO_2^{\cdot}$-$RO_2^{\cdot}$ termination

356   is contingent upon the probability of the molecular collision between the $RO_2^{\cdot}$ molecules occurring

357   before other radical termination (i.e., $RO_2^{\cdot}-NO_x$, or $RO_2^{\cdot}$-$HO_2^{\cdot}$. There is likely a strong diurnal

358   sequence in the dominant $RO_2^{\cdot}$ termination mechanisms across the day period, and the combination

359   of the two factors discussed above results in there being no strong diurnal trend in these molecules.

360   A lower oxidant concentration at night results in less $RO_2^{\cdot}$ molecules, but less NO and $HO_2^{\cdot}$ results

361   in a greater chance for those $RO_2^{\cdot}$ molecules to dimerize. As the levels of NO_x in Beijing fall, the

362   peroxy radical termination reactions will be less probable compared to continued autoxidation

363   (Praske et al., 2018), and it is expected that more oxidised HOM products will be seen with lower

364   volatilities and therefore a greater potential contribution to earlier stage particle formation and

365   growth.

366

3.3.   New Particle Formation

368   Nearly all the signal intensity in the CI-APi-ToF instrument arises from molecules charged by NO_3^-,

369   therefore plotting the unit mass data against time describes simply the evolution of oxidised organic

370   molecules, acids and their molecular clusters both with each other and stabilising amine species.

371   This is done in Figure 5. As the signal intensity varies by factors of 10 from mass to mass, all

372   masses have been normalised to 1. This has been done separately for two days for clarity, as the

373   signal intensity also varies from day to day. PSM data for these two days is plotted in Figure 5 also,

374   with both total particle count >1.30 nm in black and the number difference between the lower and

375   upper size cuts (1.30 and 1.84 nm) in blue, which shows the number of particles between these

376   sizes. The relationship between mass and electrical mobility diameter can be defined thus (Tammet,

377   1995),

378

379
$$d_e = \left(\frac{6m}{\pi\rho}\right)^{\frac{1}{3}} + d_g \qquad (3)$$

15

380

381   where d_e is the electrical mobility diameter of the cluster or particle, m is the mass of the cluster or

382   particle expressed in kg, ρ is the density and d_g is the effective gas diameter, determined to be 0.3

383   nm for smaller particles (Larriba et al., 2011). We can use this to draw a comparison between the

384   PSM and CI-APi-ToF measurements. If a density of 1.2 g cm^{-3} is assumed, then once molecular

385   clusters reach the >400 m/Q range, they will be seen in the lowest size cut of the PSM, or >700 m/Q

386   if a density of 2.0 g cm^{-3} is assumed. A full table of densities is provided in the Supplementary

387   Information.

388

389   A burst in the signal seen by the CI-APi-TOF occurs first in the late morning in the top panel of

390   Figure 5, and this is at the same time as peaks begin to rise in the identified HOMs (see Figure 3).

391   Here, the PSM is not available due to an instrumental fault until 16:00; however, at that point, an

392   elevation to particle count and a large elevation to cluster count can be seen. Moving into the

393   evening period, the mass contour shows peaks to larger masses >400 m/Q. This is likely dimerized

394   compounds and NO_3^- chemistry with little contribution to newly forming particles, but still sensitive

395   to chemical ionisation by NO_3^-. Many of these peaks cannot be assigned due to uncertainties in the

396   structural formula assignment for higher mass peaks, as the number of possible dimerised

397   compounds is many, being the combination of most possible RO_2 radicals. Graphically, these are

398   over-represented in Figure 5 due to the normalisation, their concentrations (especially >500 m/Q)

399   are much lower than the concentrations <400 m/Q.

400

401   The second day plotted in the lower panel of Figure 5 (25/06/2017) shows a strong afternoon peak

402   to the HOMs (for most HOMs, stronger than that on the day prior). Particle formation is shown in

403   the PSM data. A strong midday peak to particle number is seen with two distinct peaks to cluster

404   count. These two peaks are not coincidental with the two peaks to HOM concentrations (Figure 3)

405   nor the two peaks in aromatic VOCs (i.e., C_2-benzenes in Figure 4). Sulfuric acid, however, does

Atmospheric
Chemistry
and Physics
Discussions

406   peak synchronously with the particle number count. Sulfuric acid is plotted across the contour plot

407   in Figure 6, where PSM data is also shown in the bottom panel. The peak to CI-APi-TOF mass,

408   visible in Figure 5 occurs at around 12:00/13:00, peaks in the PSM cluster count occur at 10:00 and

409   13:00 - at 13:00 the peaks in mass occur between 200-550 m/Q. Assuming the density of the

410   identified species is ≤ 1.6 g cm^{-3} then these will be suitably sized to be grown in the PSM saturator

411   above the size cut at 1.30 nm. The peak at 10:00 in PSM cluster count is characterised by a few

412   peaks at specific masses (around 680, 720, 840, 860 m/Q), presumably specific nucleating inorganic

413   clusters, pointing towards a possible evolution in the composition of clusters throughout the

414   nucleation event with the early nucleation linked with a few specific precursors. These newly

415   formed particles then go on to grow and contribute significantly to the larger particle count (Figure

416   S3). As initial particle formation coincides with sulfuric acid concentrations and before HOM

417   concentrations peak, it can be assumed on these days, the HOM contribution to the initial particle

418   formation is modest.

419

420   There is recent strong evidence to suggest that the driving force of the earliest stages of particle

421   formation in urban Shanghai is from sulfuric acid and C$_2$-amines (Yao et al., 2018), supported by

422   the coincidental peaks of sulfuric acid with new particles as seen in Figure 6. Dimethylamine

423   (DMA) can efficiently stabilise the sulfuric acid clusters (Almeida et al., 2013). Here, few larger

424   sulfuric acid-DMA clusters were visible in the dataset, as seen in the work by Yao et al., 2018,

425   although five SA-DMA ions were observed, the others were likely too low in signal to be

426   confidently resolved from their neighbouring peaks. The scarcity of sulfuric acid-DMA clusters is

427   likely due to instrumental conditions, rather than their absence in the atmosphere. The nitrate

428   chemical ionisation system tends to evaporate amine compounds upon charging, and as specific

429   voltage-tuning setups can lend themselves towards preservation or breakage of molecular clusters,

430   the signal for larger sulfuric acid clusters was also very weak. The formation of HOM-sulfuric acid

431   clusters is unlikely under atmospheric conditions (Elm et al., 2017) and few of these were observed.

432 Concentrations of HOMs seem to coincide with later particle growth; it can be expected that HOM

433 molecules make a more significant contribution to particle growth than to early particle formation,

434 with the largest and most oxidised being involved in early growth, and the smaller and less oxidised

435 contributing to later growth as the necessary vapour pressure properties become less demanding.

436

437 **4.   CONCLUSIONS**

438 The average degree of HOM oxidation in Beijing is comparable with that seen in other

439 environments. Rapid intramolecular hydrogen shifts during autoxidation due to the higher

440 temperatures are probably offset by the frequent termination reactions due to high NO_x

441 concentrations. OS_c values seem to be marginally higher for biogenic species.

442

443 The temporal trend of nearly every HOM shows a daytime maximum. Both O_3 and $OH^.$ have high

444 daytime concentrations and these likely drive the initial oxidation steps. The species arising from

445 alkylbenzene precursors show sharper afternoon peaks, probably since their oxidation is $OH^.$

446 dominated. Many of the rest of the peaks, coming from largely BVOC precursors show broader

447 daytime peaks, being influenced by O_3 also. There seems to be no direct link between VOC

448 concentrations and HOM concentrations, with days of lower precursor VOC sometimes having

449 higher HOM concentrations and vice versa.

450

451 Initial particle formation coincides with peak sulfuric acid concentrations, while the growth of the

452 particles correlates more closely with the concentrations of HOMs. This is very similar to behaviour

453 observed in a study of NPF in Shanghai which was attributed to sulphuric acid-dimethylamine-

454 water nucleation with condensing organic species contributing to particle growth (Yao et al., 2018).

455 The freshly formed particles grow and contribute significantly to total particle loading. This is

456 visible when the unit mass CI-APi-ToF data is plotted as a contour plot, and further to this is visible

457 in the PSM data, with bursts to both total number count >1.30 nm and the number of molecular

Atmospheric
Chemistry
and Physics
Discussions

458   clusters between 1.30 and 1.84 nm. As NO_x levels fall in Beijing due to traffic emission control

459   measures being enforced it is likely that autoxidation will become increasingly significant in the

460   new particle formation processes. The number of molecules detected by the NO_3^- CIMS is

461   undoubtedly many more than have had formulae assigned here, but to identify more requires a more

462   sophisticated data deconvolution.

463

464   **DATA ACCESSIBILITY**

465   Data supporting this publication are openly available from the UBIRA eData repository at

466   https://doi.org/10.25500/edata.bham.00000304

467

468   **AUTHOR CONTRIBUTIONS**

469   The study was conceived and planned by RMH and ZS. DCSB and JB set up and operated the

470   main instrumental measurements, and JB prepared the first draft of the paper and responded to

471   comments from RMH and ZS. CNH and WJA contributed the hydrocarbon data and provided

472   comments on the draft manuscript.

473

474   **COMPETING INTERESTS**

475   The authors have no conflict of interests.

476

477   **ACKNOWLEDGMENTS**

484   Mullinger and other staff from the Centre for Ecology and Hydrology, Edinburgh for assistance

485   with the VOC measurements and associated infrastructure.

486

Atmospheric
Chemistry
and Physics
Discussions

REFERENCES

Alam, A., Shi, J.P., Harrison R.M.: Observations of new particle formation in urban air, J. Geophys. Res., 108, 4093-4107, doi:10.1029/2001JD001417, 2003

Almeida, J., Schobesberger, S., Kürten, A., Ortega, I. K., Kupiainen-Määttä, O., Praplan, A. P., Adamov, A., Amorim, A., Bianchi, F., Breitenlechner, M., David, A., Dommen, J., Donahue, N. M., Downard, A., Dunne, E., Duplissy, J., Ehrhart, S., Flagan, R. C., Franchin, A., Guida, R., Hakala, J., Hansel, A., Heinritzi, M., Henschel, H., Jokinen, T., Junninen, H., Kajos, M., Kangasluoma, J., Keskinen, H., Kupc, A., Kurtén, T., Kvashin, A. N., Laaksonen, A., Lehtipalo, K., Leiminger, M., Leppä, J., Loukonen, V., Makhmutov, V., Mathot, S., McGrath, M. J., Nieminen, T., Olenius, T., Onnela, A., Petäjä, T., Riccobono, F., Riipinen, I., Rissanen, M., Rondo, L., Ruuskanen, T., Santos, F. D., Sarnela, N., Schallhart, S., Schnitzhofer, R., Seinfeld, J. H., Simon, M., Sipilä, M., Stozhkov, Y., Stratmann, F., Tomé, A., Tröstl, J., Tsagkogeorgas, G., Vaattovaara, P., Viisanen, Y., Virtanen, A., Vrtala, A., Wagner, P. E., Weingartner, E., Wex, H., Williamson, C., Wimmer, D., Ye, P., Yli-Juuti, T., Carslaw, K. S., Kulmala, M., Curtius, J., Baltensperger, U., Worsnop, D. R., Vehkamäki, H., and Kirkby, J.: Molecular understanding of sulphuric acid-amine particle nucleation in the atmosphere, Nature, 502, 359-363, 2013.

Atkinson, R., Aschmann, S. M., Carter, W. P. L., Winer, A. M., and Pitts, J. N.: Alkyl nitrate formation from the nitrogen oxide (NOₓ)air photooxidations of C2-C8 n-alkanes, J. Phys. Chem., 86, 4563-4569, 1982.

Berndt, T., Richters, S., Kaethner, R., Voigtländer, J., Stratmann, F., Sipilä, M., Kulmala, M., and Herrmann, H.: Gas-Phase Ozonolysis of Cycloalkenes: Formation of Highly Oxidized RO2 Radicals and Their Reactions with NO, NO2, SO2, and Other RO2 Radicals, J. Phys. Chem. A., 119, 10336-10348, 2015.

Berndt, T., Richters, S., Jokinen, T., Hyttinen, N., Kurtén, T., Otkjær, R. V., Kjaergaard, H. G., Stratmann, F., Herrmann, H., Sipilä, M., Kulmala, M., and Ehn, M.: Hydroxyl radical-induced formation of highly oxidized organic compounds, Nature Comm., 7, 20 https://doi.org/10.1038/ncomms13677, 2016.

Bianchi, F., Garmash, O., He, X., Yan, C., Iyer, S., Rosendahl, I., Xu, Z., Rissanen, M. P., Riva, M., Taipale, R., Sarnela, N., Petäjä, T., Worsnop, D. R., Kulmala, M., Ehn, M., and Junninen, H.: The role of highly oxygenated molecules (HOMs) in determining the composition of ambient ions in the boreal forest, Atmos. Chem. Phys., 17, 13819-13831, 2017.

Bohn, B., Heard, D. E., Mihalopoulos, N., Plass-Dülmer, C., Schmitt, R., and Whalley, L. K.: Characterisation and improvement of j(O1D) filter radiometers, Atmos. Meas. Tech., 9, 3455-3466, 2016.

Brook, R. D., Rajagopalan, S., Pope, C. A., Brook, J. R., Bhatnagar, A., Diez-Roux, A. V., Holguin, F., Hong, Y., Luepker, R. V., Mittleman, M. A., Peters, A., Siscovick, D., Smith, S. C., Whitsel, L., and Kaufman, J. D.: Particulate matter air pollution and cardiovascular disease: An update to the scientific statement from the american heart association, Circulation, 121, 2331-2378, 2010.

Chu, B., Kerminen, V.-M., Bianchi, F., Yan, C., Petaja, T., and Kulmala, M.: Atmospheric new particle formation in China, Atmos. Chem. Phys., 19, 115-138, 2019.

Crounse, J. D., Nielsen, L. B., Jørgensen, S., Kjaergaard, H. G., and Wennberg, P. O.: Autoxidation of organic compounds in the atmosphere, J. Phys. Chem. Lett., 4, 3513-3520, 2013.

Atmospheric
Chemistry
and Physics
Discussions

539 Cubison, M. J. and Jimenez, J. L.: Statistical precision of the intensities retrieved from constrained
540 fitting of overlapping peaks in high resolution mass spectra, Atmos. Meas. Tech., 8, 2333-2345,
541 2015.
542
543 Delfino, R. J., Sioutas, C., and Malik, S.: Potential role of ultrafine particles in associations between
544 airborne particle mass and cardiovascular health, Environ. Health Perspect., 113, 934-946, 2005.
545
546 Ehn, M., Thornton, J. A., Kleist, E., Sipilä, M., Junninen, H., Pullinen, I., Springer, M., Rubach, F.,
547 Tillmann, R., Lee, B., Lopez-Hilfiker, F., Andres, S., Acir, I.-H., Rissanen, M., Jokinen, T.,
548 Schobesberger, S., Kangasluoma, J., Kontkanen, J., Nieminen, T., Kurtén, T., Nielsen,
549 L. B., Jørgensen, S., Kjaergaard, H. G., Canagaratna, M., Maso, M. D., Berndt, T., Petäjä, T.,
550 Wahner, A., Kerminen, V.-M., Kulmala, M., Worsnop, D. R., Wildt, J., and Mentel, T. F.: A large
551 source of low-volatility secondary organic aerosol, Nature, 506, 476-479, 2014.
552
553 Elm, J., Myllys, N., and Kurtén, T.: What is Required for Highly Oxidized Molecules to Form
554 Clusters with Sulfuric Acid?, J. Phys. Chem. A, 121, 4578-4587, 2017.
555
556 Gong, Y., Hu, M., Cheng, Y., Su, H., Yue, D., Liu, F., Wiedensohler, A., Wang, Z., Kalesse, H.,
557 Liu, S., Wu, Z., Xiao, K., Mi, P., and Zhang, Y.: Competition of coagulation sink and source rate:
558 New particle formation in the Pearl River Delta of China, Atmos. Environ., 44, 3278-3285, 2010.
559
560 Guo, S., Hu, M., Zamora, M. L., Peng, J., Shang, D., Zheng, J., Du, Z., Wu, Z., Shao, M., Zeng, L.,
561 Molina, M. J., and Zhang, R.: Elucidating severe urban haze formation in China., PNAS, 111,
562 17373- 17378, 2014.
563
564 Hyttinen, N., Kupiainen-Määttä, O., Rissanen, M. P., Muuronen, M., Ehn, M., and Kurtén, T.:
565 Modeling the Charging of Highly Oxidized Cyclohexene Ozonolysis Products Using Nitrate-Based
566 Chemical Ionization, J. Phys. Chem., A, 119, 6339-6345, 2015.
567
568 Isaacman-Vanwertz, G., Massoli, P., O'Brien, R., Lim, C., Franklin, J. P., Moss, J. A., Hunter, J. F.,
569 Nowak, J. B., Canagaratna, M. R., Misztal,P. K., Arata, C., Roscioli, J. R., Herndon, S. T., Onasch,
570 T. B., Lambe, A. T., Jayne, J. T., Su, L., Knopf, D. A., Goldstein, A. H., Worsnop, D. R., and Kroll,
571 J. H.: Chemical evolution of atmospheric organic carbon over multiple generations of oxidation,
572 Nature Chem., 10,462-468, https://doi.org/10.1038/s41557-018-0002-2, 2018
573
574 Jokinen, T., Sipilä, M., Junninen, H., Ehn, M., Lönn, G., Hakala, J., Petäjä, T., Mauldin, R. L.,
575 Kulmala, M., and Worsnop, D. R.: Atmospheric sulphuric acid and neutral cluster measurements
576 using CI-APi-TOF, Atmos. Chem. Phys., 12, 4117-4125, 2012.
577
578 Jokinen, T., Sipilä, M., Richters, S., Kerminen, V. M., Paasonen, P., Stratmann, F., Worsnop, D.,
579 Kulmala, M., Ehn, M., Herrmann, H., and Berndt, T.: Rapid autoxidation forms highly oxidized
580 RO2 radicals in the atmosphere, Angewandte Chemie - International Edition, 53, 14596-14600,
581 https://doi.org/10.1002/anie.201408566, 2014.
582
583 Junninen, H., Ehn, M., Petäjä, Luosujärvi, L., Kotiaho, T., Kostiainen, R., Rohner, U., Gonin, M.,
584 Fuhrer, K., Kulmala, M., and Worsnop, D. R.: A high-resolution mass spectrometer to measure
585 atmospheric ion composition, Atmos. Meas. Tech., 3, 1039-1053, 2010.
586
587 Kerminen, V. M., Paramonov, M., Anttila, T., Riipinen, I., Fountoukis, C., Korhonen, H., Asmi, E.,
588 Laakso, L., Lihavainen, H., Swietlicki, E., Svenningsson, B., Asmi, A., Pandis, S. N., Kulmala, M.,
589 and Petäjä, T.: Cloud condensation nuclei production associated with atmospheric nucleation: A

590 synthesis based on existing literature and new results, Atmos. Chem. Phys., 12, 12037-12059, 2012.
591
592 Khan, M., Cooke M, Utembe, S., Archibald A., Derwent, R., Jenkin, M., Morris, W., South, N.,
593 Hansen, J., Francisco, J., Percival, C., Shallcross, D.: Global analysis of peroxy radicals and peroxy
594 radical-water complexation using the STOCHEM-CRI global chemistry and transport model,
595 Atmos. Environ., 106, 278-287, 2015.
596
597 Kirkby, J., Curtius, J., Almeida, J., Dunne, E., Duplissy, J., Ehrhart, S., Franchin, A., Gagné, S.,
598 Ickes, L., Kürten, A., Kupc, A., Metzger, A., Riccobono, F., Rondo, L., Schobesberger, S.,
599 Tsagkogeorgas, G., Wimmer, D., Amorim, A., Bianchi, F., Breitenlechner, M., David, A.,
600 Dommen, J., Downard, A., Ehn, M., Flagan, R. C., Haider, S., Hansel, A., Hauser, D., Jud, W.,
601 Junninen, H., Kreissl, F., Kvashin, A., Laaksonen, A., Lehtipalo, K., Lima, J., Lovejoy, E. R.,
602 Makhmutov, V., Mathot, S., Mikkilä, J., Minginette, P., Mogo, S., Nieminen, T., Onnela, A.,
603 Pereira, P., Petäjä, T., Schnitzhofer, R., Seinfeld, J. H., Sipilä, M., Stozhkov, Y., Stratmann, F.,
604 Tomé, A., Vanhanen, J., Viisanen, Y., Vrtala, A., Wagner, P. E., Walther, H., Weingartner, E.,
605 Wex, H., Winkler, P. M., Carslaw, K. S., Worsnop, D. R., Baltensperger, U., and Kulmala, M.:
606 Role of sulphuric acid, ammonia and galactic cosmic rays in atmospheric aerosol nucleation,
607 Nature, 476, 429-435, https://doi.org/10.1038/nature10343, 2011.
608
609 Kirkby, J., Duplissy, J., Sengupta, K., Frege, C., Gordon, H., Williamson, C., Heinritzi, M., Simon,
610 M., Yan, C., Almeida, J., Trostl, J., Nieminen, T., Ortega, I. K., Wagner, R., Adamov, A., Amorim,
611 A., Bernhammer, A. K., Bianchi, F., Breitenlechner, M., Brilke, S., Chen, X., Craven, J., Dias, A.,
612 Ehrhart, S., Flagan, R. C., Franchin, A., Fuchs, C., Guida, R., Hakala, J., Hoyle, C. R., Jokinen, T.,
613 Junninen, H., Kangasluoma, J., Kim, J., Krapf, M., Kurten, A., Laaksonen, A., Lehtipalo, K.,
614 Makhmutov, V., Mathot, S., Molteni, U., Onnela, A., Perakyla, O., Piel, F., Petaja, T., Praplan, A.
615 P., Pringle, K., Rap, A., Richards, N. A., Riipinen, I., Rissanen, M. P., Rondo, L., Sarnela, N.,
616 Schobesberger, S., Scott, C. E., Seinfeld, J. H., Sipila, M., Steiner, G., Stozhkov, Y., Stratmann, F.,
617 Tomé, A., Virtanen, A., Vogel, A. L., Wagner, A. C., Wagner, P. E., Weingartner, E., Wimmer, D.,
618 Winkler, P. M., Ye, P., Zhang, X., Hansel, A., Dommen, J., Donahue, N. M., Worsnop, D. R.,
619 Baltensperger, U., Kulmala, M., Carslaw, K. S., and Curtius, J.: Ion-induced nucleation of pure
620 biogenic particles, Nature, 533, 521-526, https://doi.org/10.1038/nature17953, 2016.
621
622 Kroll, J. H., Donahue, N. M., Jimenez, J. L., Kessler, S. H., Canagaratna, M. R., Wilson, K. R.,
623 Altieri, K. E., Mazzoleni, L. R., Wozniak, A. S., Bluhm, H., Mysak, E. R., Smith, J. D., Kolb, C. E.,
624 and Worsnop, D. R.: Carbon oxidation state as a metric for describing the chemistry of atmospheric
625 organic aerosol, Nature Chemistry, 3, 133-139, https://doi.org/10.1038/nchem.948, 2011.
626
627 Kulmala, M., Petäjä, T., Mönkkönen, P., Koponen, I. K., Dal Maso, M., Aalto, P. P., Lehtinen, K.
628 E. J., and Kerminen, V.-M.: On the growth of nucleation mode particles: source rates of
629 condensable vapor in polluted and clean environments, Atmos. Chem. Phys., 5, 409-416, 2005.
630
631 Kulmala, M., Petäjä, T., Nieminen, T., Sipilä, M., Manninen, H. E., Lehtipalo, K., Dal Maso, M.,
632 Aalto, P. P., Junninen, H., Paasonen, P.,Riipinen, I., Lehtinen, K. E. J., Laaksonen, A., and
633 Kerminen, V.-M.: Measurement of the nucleation of atmospheric aerosol particles, Nature
634 Protocols, 7, 1651-1667, https://doi.org/10.1038/nprot.2012.091, 2012.
635
636 Kurtén, T., Rissanen, M. P., Mackeprang, K., Thornton, J. A., Hyttinen, N., Jørgensen, S., Ehn, M.,
637 and Kjaergaard, H. G.: Computational Study of Hydrogen Shifts and Ring-Opening Mechanisms in
638 α-Pinene Ozonolysis Products, J. Phys. Chem., A, 119, 11366-11375, 2015.
639
640

641   Kurtén, T., Tiusanen, K., Roldin, P., Rissanen, M., Luy, J. N., Boy, M., Ehn, M., and Donahue, N.:
642   α-Pinene autoxidation products may not have extremely low saturation vapor pressures despite high
643   O:C ratios, J. Phys. Chem., A, 120, 2569-2582, 2016.
644
645   Larriba, C., Hogan, C. J., Attoui, M., Borrajo, R., Garcia, J. F., and De La Mora, J. F.: The
646   mobility-volume relationship below 3.0 nm examined by tandem mobility-mass measurement,
647   Aerosol Sci.Techn., 45, 453-467, 2011.
648
649   Lee, B. H., Mohr, C., Lopez-Hilfiker, F. D., Lutz, A., Hallquist, M., Lee, L., Romer, P., Cohen, R.
650   C., Iyer, S., Kurtén, T., Hu, W., Day, D. A., Campuzano-Jost, P., Jimenez, J. L., Xu, L., Ng, N. L.,
651   Guo, H., Weber, R. J., Wild, R. J., Brown, S. S., Koss, A., de Gouw, J., Olson, K., Goldstein, A. H.,
652   Seco, R., Kim, S., McAvey, K., Shepson, P. B., Starn, T., Baumann, K., Edgerton, E. S., Liu, J.,
653   Shilling, J. E., Miller, D. O., Brune, W., Schobesberger, S., D'Ambro, E. L., and Thornton, J. A.:
654   Highly functionalized organic nitrates in the southeast United States: Contribution to secondary
655   organic aerosol and reactive nitrogen budgets, PNAS, 113, 1516-1521, 2016.
656
657   Lehtipalo, K., Yan, C., Dada, L., Bianchi, F., Xiao, M., Wagner,R., Stolzenburg, D., Ahonen, L. R.,
658   Amorim, A., Baccarini, A.,5Bauer, P. S., Baumgartner, B., Bergen, A., Bernhammer, A.-
659   K.,Breitenlechner, M., Brilke, S., Buchholz, A., Mazon, S. B., Chen,D., Chen, X., Dias, A.,
660   Dommen, J., Draper, D. C., Duplissy,J., Ehn, M., Finkenzeller, H., Fischer, L., Frege, C., Fuchs,
661   C.,Garmash, O., Gordon, H., Hakala, J., He, X., Heikkinen, L.,Heinritzi, M., Helm, J. C., Hofbauer,
662   V., Hoyle, C. R., Joki-nen, T., Kangasluoma, J., Kerminen, V.-M., Kim, C., Kirkby,J., Kontkanen,
663   J., Kürten, A., Lawler, M. J., Mai, H., Mathot,S., Mauldin, R. L., Molteni, U., Nichman, L., Nie,
664   W., Niemi-nen, T., Ojdanic, A., Onnela, A., Passananti, M., Petäjä, T., Piel,15F., Pospisilova, V.,
665   Quéléver, L. L. J., Rissanen, M. P., Rose,C., Sarnela, N., Schallhart, S., Schuchmann, S., Sengupta,
666   K.,Simon, M., Sipilä, M., Tauber, C., Tomé, A., Tröstl, J., Väisä-nen, O., Vogel, A. L., Volkamer,
667   R., Wagner, A. C., Wang, M.,Weitz, L., Wimmer, D., Ye, P., Ylisirniö, A., Zha, Q., Carslaw, K. S.,
668   Curtius, J., Donahue, N. M., Flagan, R. C., Hansel, A.,Riipinen, I., Virtanen, A., Winkler, P. M.,
669   Baltensperger, U., Kulmala, M., and Worsnop, D. R.: Multicomponent new particle formation from
670   sulfuric acid, ammonia, and biogenic vapors, Science Advances, 4,
671   https://doi.org/10.1126/sciadv.aau5363, 2018.
672
673   Massoli, P., Stark, H., Canagaratna, M. R., Krechmer, J. E., Xu, L., Ng, N. L., Mauldin, R. L., Yan,
674   C., Kimmel, J., Misztal, P. K., Jimenez, J. L., Jayne, J. T., and Worsnop, D. R.: Ambient
675   Measurements of Highly Oxidized Gas-Phase Molecules during the Southern Oxidant and Aerosol
676   Study (SOAS) 2013, ACS Earth Space Chem.,, 2, 653-672, 2018.
677
678   McMurry, P. H., Shan Woo, K., Weber, R., Chen, D.-R., and Pui, D. Y. H.: Size distributions of 3-
679   10 nm atmospheric particles: implications for nucleation mechanisms, Philosophical Transactions
680   of the Royal Society A: Math., Phys. Eng. Sci., 358, 2625-2642, 2000.
681
682   Miller, M. R., Raftis, J. B., Langrish, J. P., McLean, S. G., Samutrtai, P., Connell, S. P., Wilson, S.,
683   Vesey, A. T., Fokkens, P. H., Boere, A. J. F., Krystek, P., Campbell, C. J., Hadoke, P. W.,
684   Donaldson, K., Cassee, F. R., Newby, D. E., Duffin, R., and Mills, N. L.: Inhaled nanoparticles
685   accumulate at sites of vascular disease, ACS Nano, 11, 4542-4552, 2017.
686
687   Møller, K. H., Tram, C. M., and Kjaergaard, H. G.: Side-by-Side Comparison of Hydroperoxide
688   and Corresponding Alcohol as HydrogenBond Donors, J. Phys. Chem. A, 121, 2951-2959, 2017.
689
690
691

692 Molteni, U., Bianchi, F., Klein, F., Haddad, I. E., Frege, C., Rossi, M. J., Dommen, J., and
693 Baltensperger, U.: Formation of highly oxygenated organic molecules from aromatic compounds,
694 Atmos. Chem. Phys., 18, 1909-1921, 2018.
695
696 Mutzel, A., Poulain, L., Berndt, T., Iinuma, Y., Rodigast, M., Böge, O., Richters, S., Spindler, G.,
697 Sipila, M., Jokinen, T., Kulmala, M., Herrmann, H.: Highly oxidized multifunctional organic
698 compounds observed in tropospheric particles: A field and laboratory study, Environ. Sci. Techn.,
699 49, 7754-7761, 2015.
700
701 Myllys, N., Olenius, T., Kurtén, T., Vehkamäki, H., Riipinen, I., and Elm, J.: Effect of Bisulfate,
702 Ammonia, and Ammonium on the Clustering of Organic Acids and Sulfuric Acid, J. Phys. Chem.
703 A, 121, 4812-4824, 2017.
704
705 Penner, J. E., Xu, L., and Wang, M.: Satellite methods underestimate indirect climate forcing by
706 aerosols., PNAS, 108, 13404-13408, 2011.
707
708 Praske, E., Otkjær, R. V., Crounse, J. D., Hethcox, J. C., Stoltz, B. M., Kjaergaard, H. G., and
709 Wennberg, P. O.: Atmospheric autoxidation is increasingly important in urban and suburban North
710 America, PNAS, 115, 64-69, 2018.
711
712 Qi, X., Ding, A., Roldin, P., Xu, Z., Zhou, P., Sarnela, N., Nie, W., Huang, X., Rusanen, A., Ehn,
713 M., Rissanen, M. P., Petäjä, T., Kulmala, M., and Boy, M.: Modelling studies of HOMs and their
714 contributions to new particle formation and growth: comparison of boreal forest in Finland and a
715 polluted environment in China, Atmos. Chem. Phys, 18, 11779-11791, 2018.
716
717 Quéléver, J., Kristensen, K., Normann Jensen, L.,Teiwes, R., Daellenbach, Kaspar R ., Peräkylä, O.,
718 Roldin, P., Pedersen, H., Glasius, M., Bilde, M., Ehn, M.: Effect of temperature on the formation of
719 Highly-oxygenated Organic Molecules (HOM) from alpha-pinene ozonolysis, Atmos. Chem. Phys.
720 Discuss., 18, 1-29, 2018.
721
722 Riccobono, F., Schobesberger, S., Scott, C., Dommen, J., Ortega, I., Rondo, L., Almeida, J.,
723 Amorim, A., Bianchi, F., Breitenlechner, M., David, A., Downard, A., Dunne, E., Duplissy, J.,
724 Ehrhart, S., Flagan, R., Franchin, A., Hansel, A., Junninen, H., Kajos, M., Keskinen, H., Kupc, A.,
725 Kürten, A., Kvashin, A., Laaksonen, A., Lehtipalo, K., Makhmutov, V., Mathot, S., Nieminen, T.,
726 Onnela, A., Petäjä, T., Praplan, A., Santos, F., Schallhart, S., Seinfeld, J., Sipilä, M., Van Spracklen,
727 D., Stozhkov, Y., Stratmann, F., Tomé, A., Tsagkogeorgas, G., Vaattovaara, P., Viisanen, Y.,
728 Vrtala, A., Wagner, P., Weingartner, E., Wex, H., Wimmer, D., Carslaw, K., Curtius, J., Donahue,
729 N., Kirkby, J., Kulmala, M., Worsnop, D., and Baltensperger, U.: Oxidation products of biogenic
730 emissions contribute to nucleation of atmospheric particles, Science, 344, 717-721, 2014.
731
732 Rissanen, M. P., Kurtén, T., Sipilä, M., Thornton, J. A., Kangasluoma, J., Sarnela, N., Junninen, H.,
733 Jørgensen, S., Schallhart, S., Kajos, M. K., Taipale, R., Springer, M., Mentel, T. F., Ruuskanen, T.,
734 Petäjä, T., Worsnop, D. R., Kjaergaard, H. G., and Ehn, M.: The formation of highly oxidized
735 multifunctional products in the ozonolysis of cyclohexene, J.Am. Chem. Soc., 136, 15596-15606
736 2014.
737
738 Rose, C., Zha, Q., Dada, L., Yan, C., Lehtipalo, K., Junninen, H., Mazon, S. B., Jokinen, T.,
739 Sarnela, N., Sipilä, M., Petäjä, T., Kerminen, V.-M., Bianchi, F., and Kulmala, M.: Observations of
740 biogenic ion-induced cluster formation in the atmosphere, Sci. Adv., 4, eaar5218,
741 https://doi.org/10.1126/sciadv.aar5218, 2018.
742
743

Atmospheric
Chemistry
and Physics
Discussions

744   Schobesberger, S., Junninen, H., Bianchi, F., Lönn, G., Ehn, M., Lehtipalo, K., Dommen, J.,
745   Ehrhart, S., Ortega, I. K., Franchin, A., Nieminen, T., Riccobono, F., Hutterli, M., Duplissy, J.,
746   Almeida, J., Amorim, A., Breitenlechner, M., Downard, A. J., Dunne, E. M., Flagan, R. C., Kajos,
747   M., Keskinen, H., Kirkby, J., Kupc, A., Kürten, A., Kurtén, T., Laaksonen, A., Mathot, S., Onnela,
748   A., Praplan, A. P., Rondo, L., Santos, F. D., Schallhart, S., Schnitzhofer, R., Sipilä, M., Tomé, A.,
749   Tsagkogeorgas, G., Vehkamäki, H., Wimmer, D., Baltensperger, U., Carslaw, K. S., Curtius, J.,
750   Hansel, A., Petäjä, T., Kulmala, M., Donahue, N. M., and Worsnop, D. R.: Molecular
751   understanding of atmospheric particle formation from sulfuric acid and large oxidized organic
752   molecules., PNAS, 110, 17223-17228, 2013.
753
754   Shi, J. P., Evans, D. E., Khan, A. A., and Harrison, R. M.: Sources and concentration of
755   nanoparticles (<10nm diameter) in the urban atmosphere, Atmos. Environ., 35, 1193-1202, 2001.
756
757   Shi, Z., Vu, T., Kotthaus, S., Grimmond, S., Harrison, R. M., Yue, S., Zhu, T., Lee, J., Han, Y.,
758   Demuzere, M., Dunmore, R. E., Ren, L., Liu, D., Wang, Y., Wild, O., Allan, J., Barlow, J.,
759   Beddows, D., Bloss, W. J., Carruthers, D., Carslaw, D. C., Chatzidiakou, L., Crilley, L., Coe, H.,
760   Dai, T., Doherty, R., Duan, F., Fu, P., Ge, B., Ge, M., Guan, D., Hamilton, J. F., He, K., Heal, M.,
761   Heard, D., Hewitt, C. N., Hu, M., Ji, D., Jiang, X., Jones, R., Kalberer, M., Kelly, F. J., Kramer, L.,
762   Langford, B., Lin, C., Lewis, A. C., Li, J., Li, W., Liu, H., Loh, M., Lu, K., Mann, G., McFiggans,
763   G., Miller, M., Mills, G., Monk, P., Nemitz, E., O'Connor, F., Ouyang, B., Palmer, P. I., Percival,
764   C., Popoola, O., Reeves, C., Rickard, A. R., Shao, L., Shi, G., Spracklen, D., Stevenson, D., Sun,
765   Y., Sun, Z., Tao, S., Tong, S., Wang, Q., Wang, W., Wang, X., Wang, Z., Whalley, L., Wu, X., Wu,
766   Z., Xie, P., Yang, F., Zhang, Q., Zhang, Y., Zhang, Y., and Zheng, M.: Introduction to Special Issue
767   – In-depth study of air pollution sources and processes within Beijing and its surrounding region
768   (APHH-Beijing), Atmos. Chem. Phys. Discuss., https://doi.org/10.5194/acp-2018-922, 2018.
769
770   Stolzenburg, D, Fischer, L., Vogel, A., Heinritzi, M., Schervish, M., Simon, M., Wagner, A.,
771   Dada, L., Ahonen, L., Amorim, A., Baccarini, A., Bauer, P., Baumgartner, B., Bergen, A.,
772   Bianchi, F., Breitenlechner, M., Brilke, S., Buenrostro Mazon, S., Chen, D., Dias, A., Draper, D.,
773   Duplissy, J., El Haddad, I., Finkenzeller, H., Frege, C., Fuchs, C., Garmash, O., Gordon, H., He, X.,
774   Helm, J., Hofbauer, V., Hoyle, C., Kim, C., Kirkby, J., Kontkanen, J., Kürten, A., Lampilahti, J.,
775   Lawler, M., Lehtipalo, K., Leiminger, M., Mai, H., Mathot, S., Mentler, B., Molteni, U., Nie, W.,
776   Nieminen, T., Nowak, J., Ojdanic, A., Onnela, A., Passananti, M., Petäjä, T., Quéléver, L.,
777   Rissanen, M., Sarnela, N., Schallhart, S., Tauber, C., Tomé, A., Wagner, R., Wang, M., Weitz, L.,
778   Wimmer, D., Xiao, M., Yan, C., Ye, P., Zha, Q., Baltensperger, U., Curtius, J., Dommen, J., Flagan,
779   R., Kulmala, M., Smith, J., Worsnop, D., Hansel, A., Donahue, N., Winkler, P., Rapid growth of
780   organic aerosol nanoparticles over a wide tropospheric temperature range, PNAS, 115, 9122-9127,
781   2018.
782
783   Tammet, H.: Size and mobility of nanometer particles, clusters and ions, J. Aerosol Sci., 26, 459-
784   475, 1995.
785
786   Tomasi, C., Fuzzi, S., Kokhanovsky, A.: Atmospheric Aerosols: Life Cycles and Effects on Air
787   Quality and Climate, Wiley, 2016.
788
789   Tröstl, J., Chuang, W. K., Gordon, H., Heinritzi, M., Yan, C., Molteni, U., Ahlm, L., Frege, C.,
790   Bianchi, F., Wagner, R., Simon, M., Lehtipalo, K., Williamson, C., Craven, J. S., Duplissy, J.,
791   Adamov, A., Almeida, J., Bernhammer, A. K., Breitenlechner, M., Brilke, S., Dias, A., Ehrhart, S.,
792   Flagan, R. C., Franchin, A., Fuchs, C., Guida, R., Gysel, M., Hansel, A., Hoyle, C. R., Jokinen, T.,
793   Junninen, H., Kangasluoma, J., Keskinen, H., Kim, J., Krapf, M., Kürten, A., Laaksonen, A.,
794   Lawler, M., Leiminger, M., Mathot, S., Möhler, O., Nieminen, T., Onnela, A., Petäjä, T., Piel, F.
795   M., Miettinen, P., Rissanen, M. P., Rondo, L., Sarnela, N., Schobesberger, S., Sengupta, K., Sipilä,

Atmospheric
Chemistry
and Physics
Discussions

796   M., Smith, J. N., Steiner, G., Tomè, A., Virtanen, A., Wagner, A. C., Weingartner, E., Wimmer, D.,
797   Winkler, P. M., Ye, P., Carslaw, K. S., Curtius, J., Dommen, J., Kirkby, J., Kulmala, M., Riipinen,
798   I., Worsnop, D. R., Donahue, N. M., and Baltensperger, U.: The role of low-volatility organic
799   compounds in initial particle growth in the atmosphere, Nature, 533, 527-531,
800   https://doi.org/10.1038/nature18271, 2016.

801

802   Wang, S., Wu, R., Berndt, T., Ehn, M., and Wang, L.: Formation of Highly Oxidized Radicals and
803   Multifunctional Products from the Atmospheric Oxidation of Alkylbenzenes, Environ. Sci. Techn.,
804   51, 8442-8449, 2017.

805

806   Wang, Z., Wu, Z., Yue, D., Shang, D., Guo, S., Sun, J., Ding, A., Wang, L., Jiang, J., Guo, H., Gao,
807   J., Cheung, H. C., Morawska, L., Keywood, M., and Hu, M.: New particle formation in China:
808   Current knowledge and further directions, Sci. Tot. Environ.,, 577, 258-266, 2016.

809

810   Wiedensohler, A., Cheng, Y. F., Nowak, A., Wehner, B., Achtelt, P., Berghof, M., Birmili, W., Wu,
811   Z. J., Hu, M., Zhu, T., Takegawa, N., Kita, K., Kondo, Y., Lou, S. R., Hofeumahaus, A., Holland,
812   F., Wahner, A., Gunthe, S. S., Rose, D., Su, H., and Pöschl, U.: Rapid aerosol particle growth and
813   increase of cloud condensation nucleus activity by secondary aerosol formation and condensation:
814   A case study for regionalair pollution in northeastern China, Journal of Geophysical Research
815   Atmospheres, 114, 1–13, https://doi.org/10.1029/2008JD010884, 2009.

816

817   Winiberg, F. A. F., Dillon, T. J., Orr, S. C., Groß, C. B. M., Bejan, I., Brumby, C. A., Evans, M. J.,
818   Smith, S. C., Heard, D. E., and Seakins, P. W.: Direct measurements of OH and other product
819   yields from the $HO_2 + CH_3C(O)O_2$ reaction, Atmos. Chem. Phys., 16, 4023-4042, 2016.

820

821   Wu, Z., Hu, M., Lin, P., Liu, S., Wehner, B., and Wiedensohler, A.: Particle number size
822   distribution in the urban atmosphere of Beijing, China, Atmos. Environ., 42, 7967-7980, 2008.

823

824   Wu, Z., Ma, N., Größ, J., Kecorius, S., Lu, K., Shang, D., Wang, Y., Wu, Y., Zeng, L., Hu, M.,
825   Wiedensohler, A., and Zhang, Y.: Thermodynamic properties of nanoparticles during new particle
826   formation events in the atmosphere of North China Plain, Atmos. Res., 188, 55-63, 2017.

827

828   Wu, Z. J., Hu, M., Liu, S., Wehner, B., Bauer, S., Ssling, a. M., Wiedensohler, a., Petäjä, T., Dal
829   Maso, M., and Kulmala, M.: New particle formation in Beijing, China: Statistical analysis of a 1-
830   year data set, J. Geophys. Res. Atmospheres, 112, D09209, https://doi.org/10.1029/2006JD007406,
831   2007.

832

833   Xiong, F., McAvey, K. M., Pratt, K. A., Groff, C. J., Hostetler, M. A., Lipton, M. A., Starn, T. K.,
834   Seeley, J. V., Bertman, S. B., Teng, A. P., Crounse, J. D., Nguyen, T. B., Wennberg, P. O., Misztal,
835   P. K., Goldstein, A. H., Guenther, A. B., Koss, A. R., Olson, K. F., De Gouw, J. A., Baumann, K.,
836   Edgerton, E. S., Feiner, P. A., Zhang, L., Miller, D. O., Brune, W. H., and Shepson, P. B.:
837   Observation of isoprene hydroxynitrates in the Southeastern United States and implications for the
838   fate of NO_x, Atmos. Chem. Phys., 15, 11257-11272, 2015 .

839

840   Yan, C., Nie, W., Äijälä, M., Rissanen, M. P., Canagaratna, M. R., Massoli, P., Junninen, H.,
841   Jokinen, T., Sarnela, N., Häme, S. A. K., Schobesberger, S., Canonaco, F., Yao, L., Prévôt, A. S.
842   H., Petäjä, T., Kulmala, M., Sipilä, M., Worsnop, D. R., and Ehn, M.: Source characterization of
843   highly oxidized multifunctional compounds in a boreal forest environment using positive matrix
844   factorization, Atmos. Chem.Phys., 16, 12715-12731, 2016.

845

846

847

848   Yao, L., Garmash, O., Bianchi, F., Zheng, J., Yan, C., Kontkanen, J., Junninen, H., Mazon, S. B.,
849   Ehn, M., Paasonen, P., Sipilä, M., Wang, M., Wang, X., Xiao, S., Chen, H., Lu, Y., Zhang, B.,
850   Wang, D., Fu, Q., Geng, F., Li, L., Wang, H., Qiao, L., Yang, X., Chen, J., Kerminen,
851   V. M., Petäjä, T., Worsnop, D. R., Kulmala, M., and Wang, L.: Atmospheric new particle formation
852   from sulfuric acid and amines in a Chinese megacity, Science, 361, 278-281, 2018.
853
854   Yu, F. and Luo, G.: Simulation of particle size distribution with a global aerosol model:
855   Contribution of nucleation to aerosol and CCN number concentrations, Atmospheric Chemistry and
856   Physics, 9, 7691-7710, 2009.
857
858   Yue, D. L., Hu, M., Zhang, R. Y., Wu, Z. J., Su, H., Wang, Z. B., Peng, J. F., He, L. Y., Huang, X.
859   F., Gong, Y. G., and Wiedensohler, A.: Potential contribution of new particle formation to cloud
860   condensation nuclei in Beijing, Atmos. Environ., 45, 6070-6077, 2011.
861
862   Zhao, Y., Wingen, L. M., Perraud, V., Greaves, J., and Finlayson-Pitts, B. J.: Role of the reaction of
863   stabilized Criegee intermediates with peroxy radicals in particle formation and growth in air, Phys.
864   Chem. Chem. Phys., 17, 12500-12514, 2015.
865

Atmospheric
Chemistry
and Physics
Discussions

866   **FIGURE LEGENDS:**

868   **Figure 1**   Oxidation state of carbon calculated as two times the oxygen to carbon ratio minus the
869   hydrogen to carbon ratio against carbon number for (colored) individual ions and (blue
870   circles) signal weighted average for each carbon number. Area and colour are both
871   proportional to the peak area for each ion

873   **Figure 2**   Kendrick mass defect plot of fitted mass spectral peaks between 200-700 mass units
874   where carbon is the Kendrick base. Kendrick mass defect can be defined as the
875   Kendrick integer mass - Kendrick mass. The size of point is proportional to the signal
876   intensity. As 1H has a positive mass defect (1.007276 Da), the upward trend along the
877   horizontal indicates increasing carbon chain length, and differences at similar masses
878   are due to increasing oxygen functionality, clustering with species such as sulfuric acid
879   (negative mass defect) and ammonia (positive mass defect), as 16O and 32S have
880   negative mass defects (15.9949 and 31.9721 Da respectively), while 14N has a positive
881   mass defect at 14.0031 Da. Here, two ions at 201 and 288 m/Q have been removed due
882   to high signal.

884   **Figure 3**   Summed time series of the concentrations of (top) all non-nitrogen containing HOMs
885   and all organonitrates identified, (middle) C5, C10 and C20 components, assumed to be
886   dominated by isoprene, monoterpene monomer and monoterpene dimers, signal for C20
887   multiplied 50 times to fit scale, and (bottom) summed C6 - C9 components, and
888   summed C11 - C18 components, assumed to be dominated by alkylbenzenes and other
889   larger components respectively.

891   **Figure 4**   Time series for the whole sampling campaign for the concentrations of (left axis) VOCs
892   as measured by PTR-ToF and (right axis) a selected HOM product associated with that
893   precursor.

895   **Figure 5**   Normalised unit mass NO3- CI-APi-ToF signal intensity on 24/06/2017 (top) and
896   25/06/2017 (bottom). Each individual unit mass was normalised to a maximum of 1.
897   Each period is normalised separately so the individual signal maxima on each day are
898   visible. The graph is plotted between 200-600 mass units, with every 10 mass units
899   averaged for simplicity. On the secondary axis is plotted PSM data, both total particle
900   count >1.30 nm (black trace) and total clusters between 1.30 and 1.84 nm (blue trace).
901   Data is plotted at 1 hour time resolution.
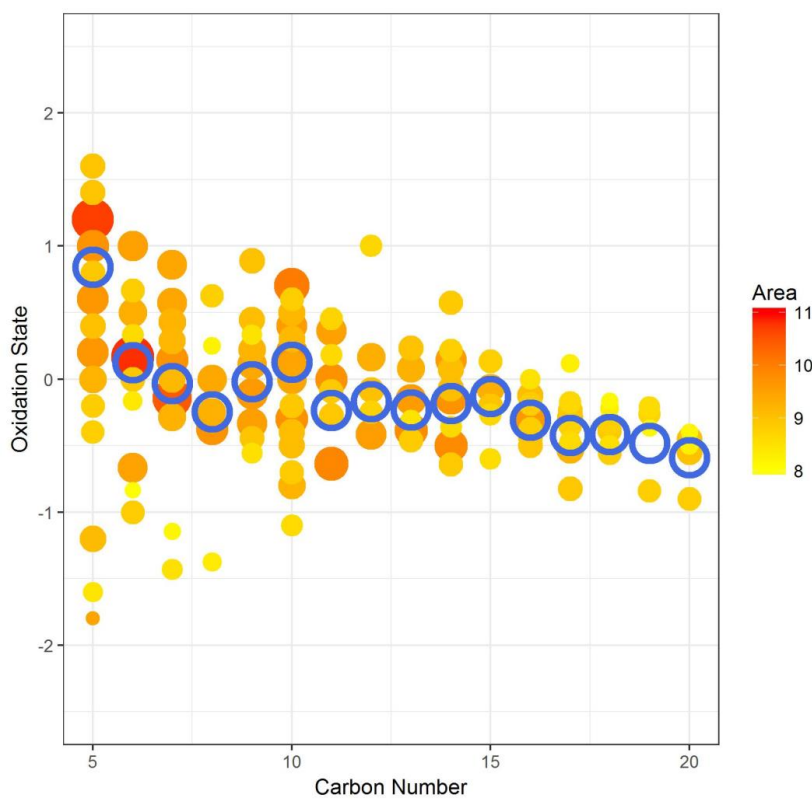
903   **Figure 6**   SMPS + PSM contour plot for two nucleation days on 24/06/2017 and 25/06/2017. Data
904   in bottom panel is from the PSM instrument, top panel from NanoSMPS, units in colour
905   bar are $\log_{10}$ ($dN/\log D_p$) for N in cm^{-3}. Points signify normalised sulfuric acid
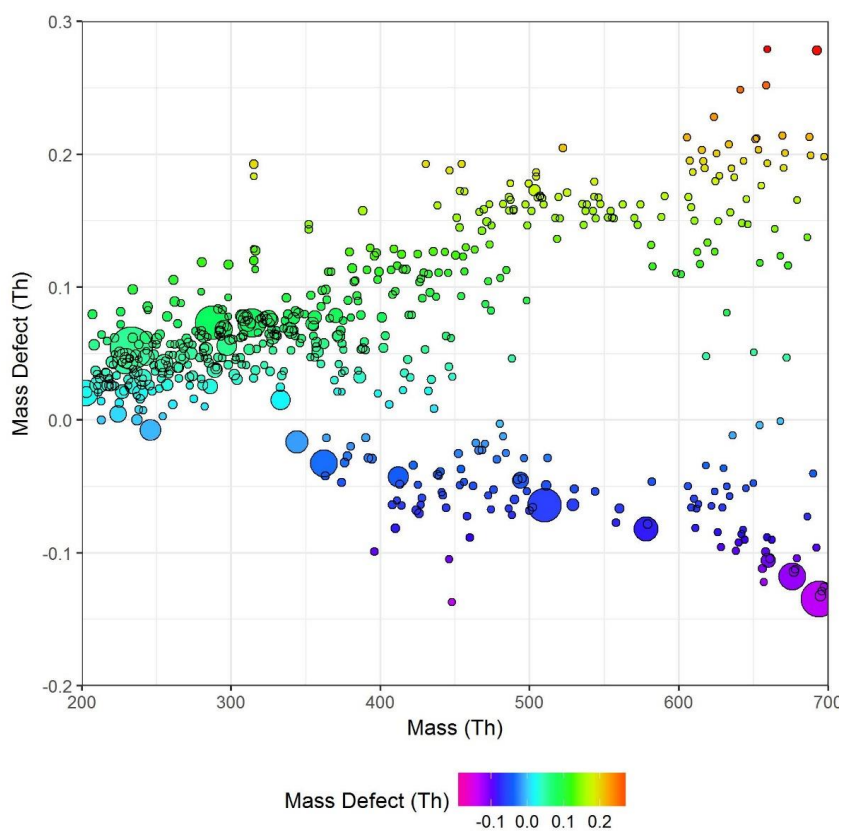906   concentration (right axis) as measured by CI-APi-ToF.

908

909

910

Figure 1. Oxidation state of carbon plotted against carbon number for (colored) individual ions and (blue circles) signal weighted average for each carbon number. Area and colour are both proportional to the peak area for each ion.

Atmospheric
Chemistry
and Physics
Discussions
Open Access

914

Figure 2. Kendrick mass defect plot of fitted mass spectral peaks between 200-700 mass units where carbon is the Kendrick base. Kendrick mass defect can be defined as the Kendrick integer mass - Kendrick mass. The size of point is proportional to the signal intensity. As ^{1}H has a positive mass defect (1.007276 Da), the upward trend along the horizontal indicates increasing carbon chain length, and differences at similar masses are due to increasing oxygen functionality, clustering with species such as sulfuric acid (negative mass defect) and ammonia (positive mass defect), as ^{16}O and ^{32}S have negative mass defects (15.9949 and 31.9721 Da respectively), while ^{14}N has a positive mass defect at 14.0031 Da. Here, two ions at 201 and 288 m/Q have been removed due to high signal.
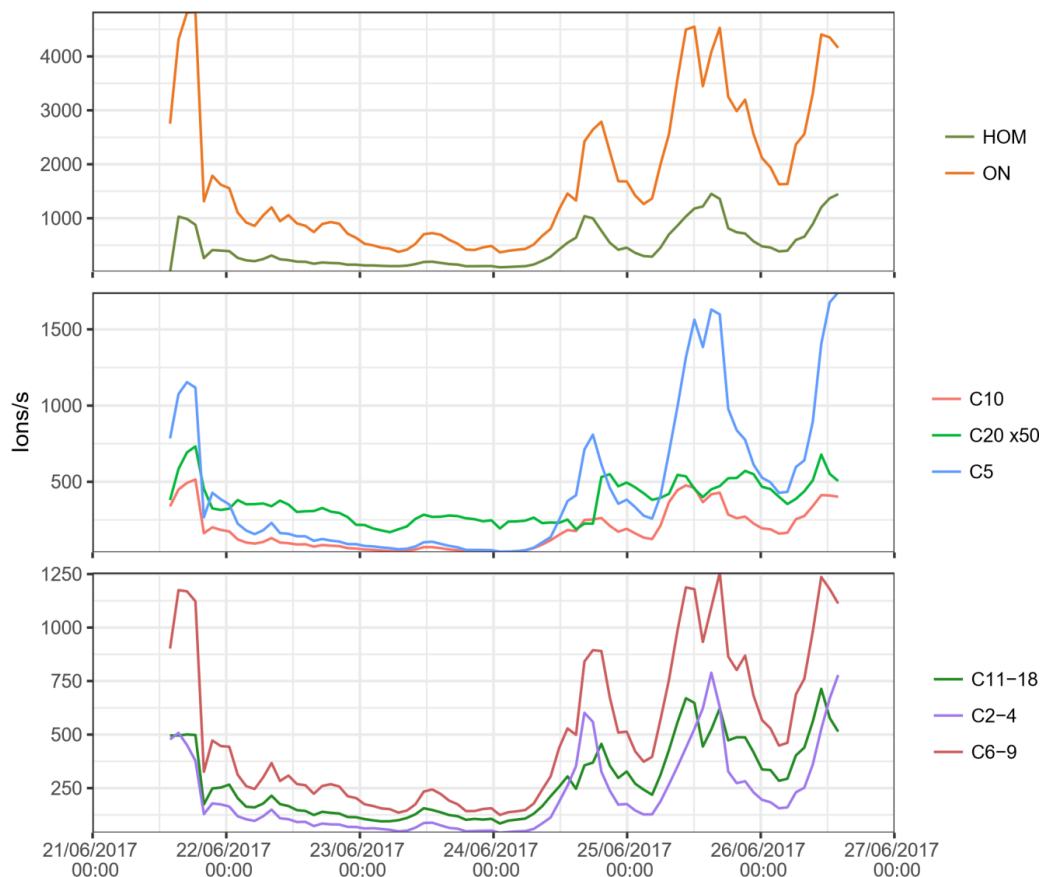
Figure 3. Summed time series of the concentrations of (top) all non-nitrogen containing HOMs and all organonitrates identified, (middle) C5, C10 and C20 components, assumed to be dominated by isoprene, monoterpene monomer and monoterpene dimers, signal for C20 multiplied 50 times to fit scale, and (bottom) summed C6 - C9 components, and summed C11 - C18 components, assumed to be dominated by alkylbenzenes and other larger components respectively.
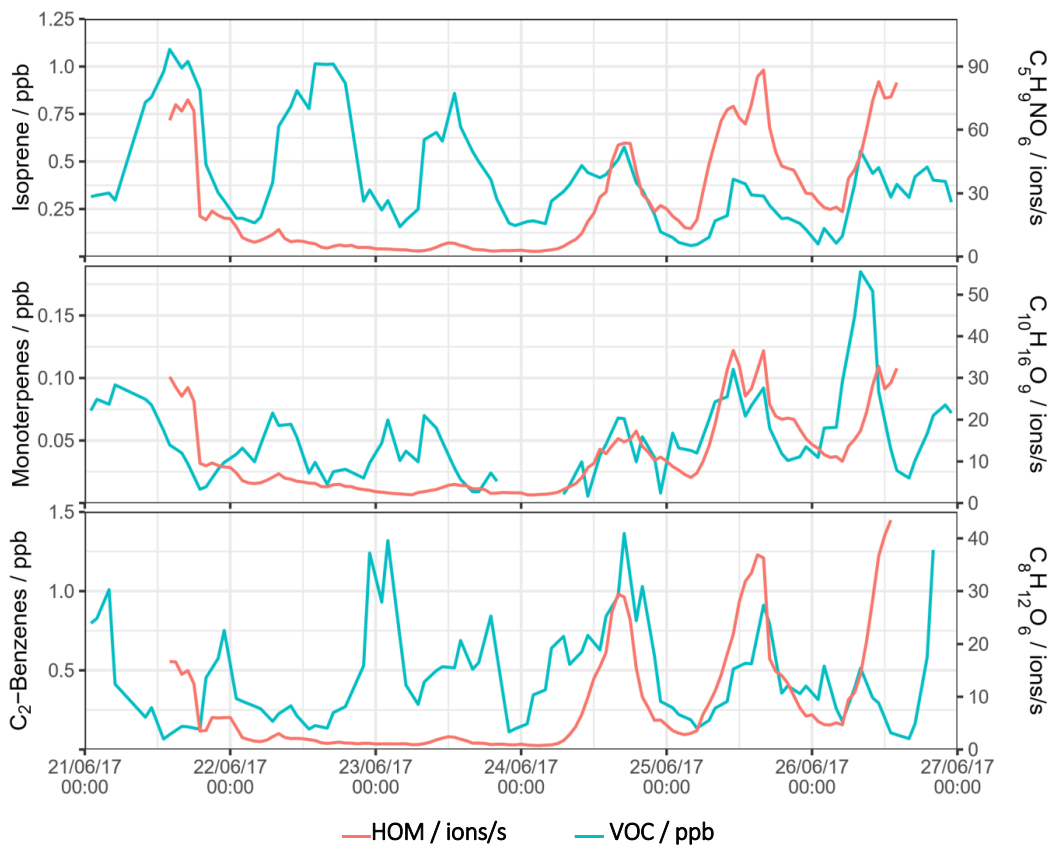
Figure 4. Time series for the whole sampling campaign for the concentrations of (left axis) VOCs as
measured by PTR-ToF and (right axis) a selected HOM product associated with that precursor.
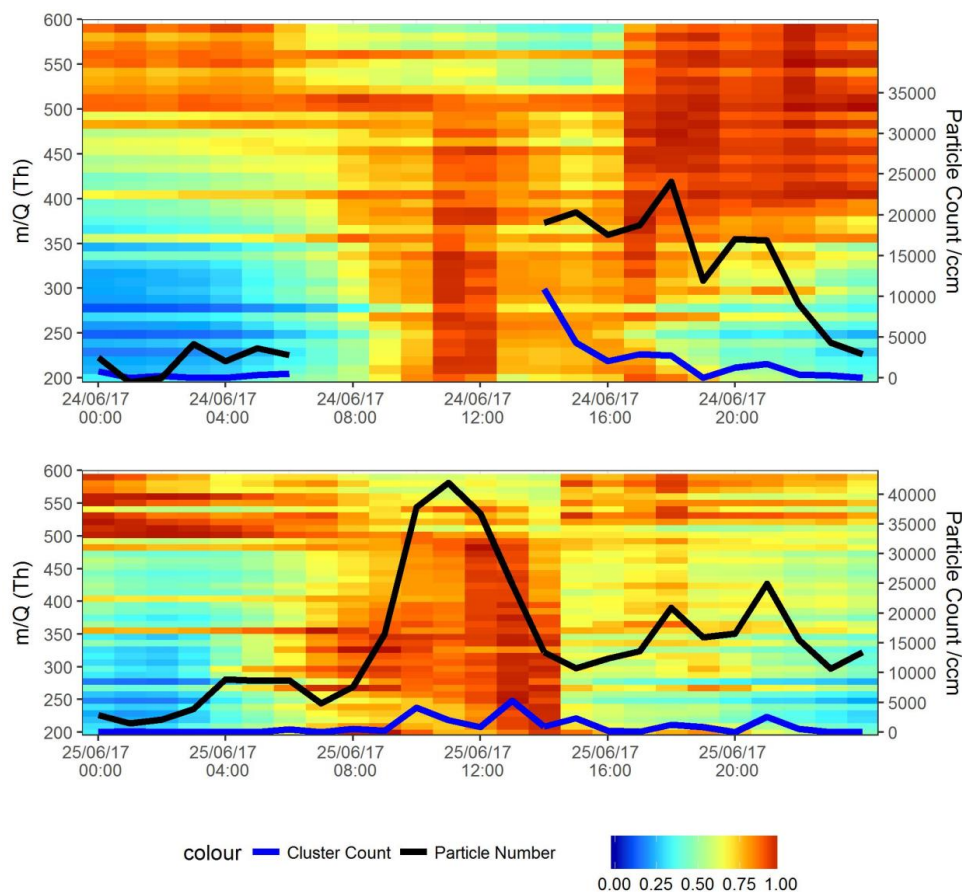
Figure 5. Normalised unit mass NO_3^- CI-APi-ToF signal intensity on 24/06/2017 (top) and 25/06/2017 (bottom). Each individual unit mass was normalised to a maximum of 1. Each period is normalised separately so the individual signal maxima on each day are visible. The graph is plotted between 200-600 mass units, with every 10 mass units averaged for simplicity. On the secondary axis is plotted PSM data, both total particle count >1.30 nm (black trace) and total clusters between 1.30 and 1.84 nm (blue trace). Data is plotted at 1 hour time resolution.
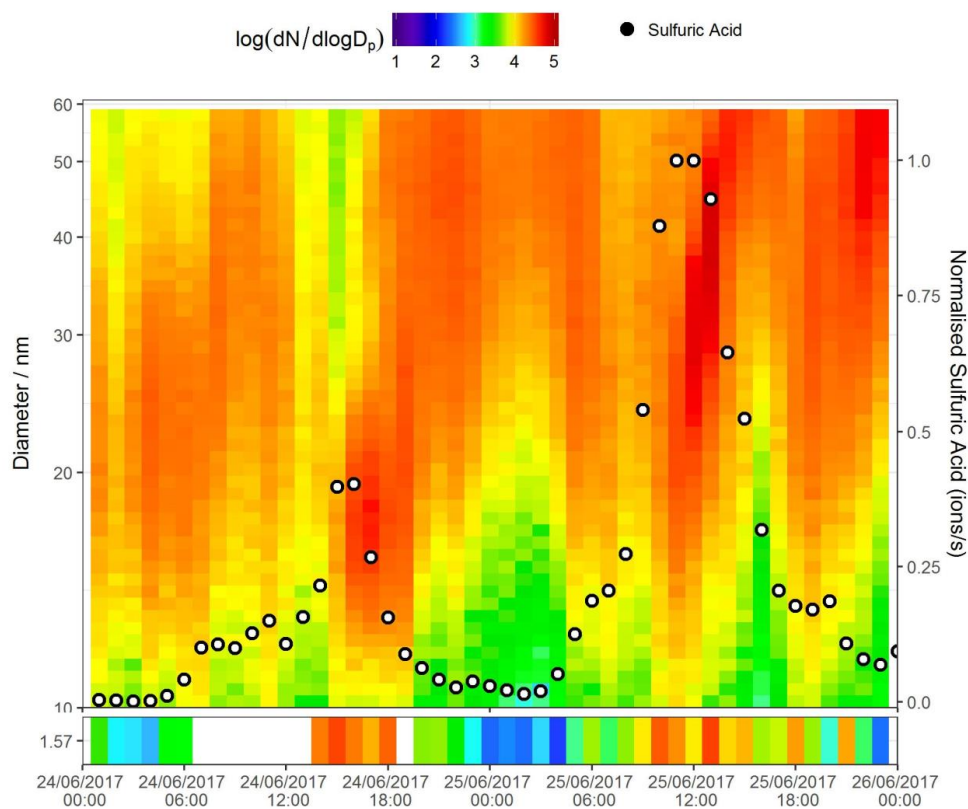
Figure 6. SMPS + PSM contour plot for two nucleation days on 24/06/2017 and 25/06/2017. Data in bottom panel is from the PSM instrument, top panel from NanoSMPS, units in colour bar are $\log_{10}$ ($dN/\log D_p$) for N in cm^{-3}. Points signify normalised sulfuric acid concentration (right axis) as measured by CI-APi-ToF.